ELSEVIER

Nuclear Instruments and Methods in Physics Research A 427 (1999) 423–436

NUCLEAR INSTRUMENTS & METHODS IN PHYSICS RESEARCH Section A

Mass discrimination using double-sided silicon microstrip detectors for pions and protons at intermediate energies

P. Bottan[a], P. Camerini[a,b], L. Celano[c], F. De Mori[a,b], M. De Palma[c,d], L. Fiore[c], N. Grion[a], V. Paticchio[c], R. Rui[a,b], L. Venturelli[e], R. Wheadon[a,*]

[a]*Instituto Nazionale di Fisica Nucleare, Sezione di Trieste, Via Valerio 2, I-34127 Trieste, Italy*
[b]*Dipartimento di Fisica dell'Universita', Via Valerio 2, I-34127 Trieste, Italy*
[c]*Instituto Nazionale di Fisica Nucleare, Via G. Amendola 173, I-70126 Bari, Italy*
[d]*Dipartimento di Fisica dell'Universita', Via G. Amendola 173, I-70126 Bari, Italy*
[e]*Dipartimento di Chimica e di Fisica per 1' Ingegneria e per i Materiali, Universitá di Brescia, Via Valotti 9, I-25123 Brescia, Italy*

Received 24 September 1998

Abstract

Prototype silicon detector modules for the vertex detector of the FINUDA experiment were tested at TRIUMF using pions and protons at 270 and 408 MeV/c in order to study their use for mass discrimination based on energy deposition. The detector modules were constructed using double-sided silicon detectors based on the ALEPH design, read out by VA1 integrated circuits. The test modules and apparatus are described, details of the data analysis are discussed, and the results are presented together with GEANT simulations. Particular attention is given to the detector response for the various particles, with signals ranging from the minimum-ionising pions at 408 MeV/c up to 20 times minimum-ionising for the protons at 270 MeV/c. © 1999 Elsevier Science B.V. All rights reserved.

PACS: 29.40.Gx; 29.40.Wk

Keywords: Silicon detector; Microstrip mass discrimination

1. Introduction

The FINUDA experiment [1] at the DAΦNE ϕ-factory, Laboratori Nazionali di Frascati, Italy [2], will study the physics of Λ-hypernuclei produced by kaons resulting from the $\phi(1020)$ resonance decaying at rest. The experiment is presently unique in nuclear physics due to the fact that it is a collider-based experiment. Thin targets are arranged in cylindrical fashion around the beam pipe, positioned between the two concentric layers of the silicon vertex detector. The internal silicon detector layer is at a radius of approximately 6.5 cm relative to the beam axis, and the external layer at approximately 8.5 cm. Negative 16 MeV kaons from the ϕ-decay pass through the first silicon layer and stop inside the targets producing hypernuclei

* Corresponding author. Tel.: + 39 40 676 3397; fax.: + 39 40 676 3350; e-mail: richard.wheadon@trieste.infn.it.

0168-9002/99/$ – see front matter © 1999 Elsevier Science B.V. All rights reserved.
PII: S0168-9002(98)01332-1

together with single "prompt" pions which have a momentum ranging from 250 to 300 MeV/c. This momentum must be measured with an accuracy of $\Delta p/p \leqslant 0.3\%$ FWHM, which is achieved by combining a precision low-mass tracking system with a strong magnetic field (1.1 T). After formation the hypernuclei decay mainly through weak channels producing protons and neutrons with an energy distribution peaking at around 70 MeV. These decay products are emitted isotropically from the decay vertex and therefore can pass either through the external silicon detector layer towards the rest of the outer tracking system or back through the internal silicon detector layer.

The vertex detector is required to

(1) Establish the $K^-(K^+)$ production, which is fully-defined by the detection of two co-linear mass-identified kaons (energy deposition up to 20 times minimum ionising) in the internal silicon detector layer.
(2) Measure the position of the interaction vertex within the nuclear target, and define with high resolution the first hit for tracks in the outer tracking system.
(3) Discriminate in both position and mass between the prompt pions and the protons resulting from the non-mesonic hypernuclear decay (which have an average energy deposition approximately six times minimum ionising).

The spatial precision required is fairly undemanding, 30 μm is more than adequate in this situation due to the limitations of multiple scattering, whereas the detectors chosen are capable of measuring with a precision of better than 10 μm. However, the strong magnetic field and the need for space point measurements from each vertex detector layer – due to the off-axis positioning of the targets – made the use of the more mature silicon microstrip detector technology preferable to that of newer techniques such as microstrip gas chambers which otherwise might have been expected to offer simpler and possibly lower-mass solutions.

2. Detector modules and readout

A schematic diagram of the detector module is shown in Fig. 1. The modules are constructed using

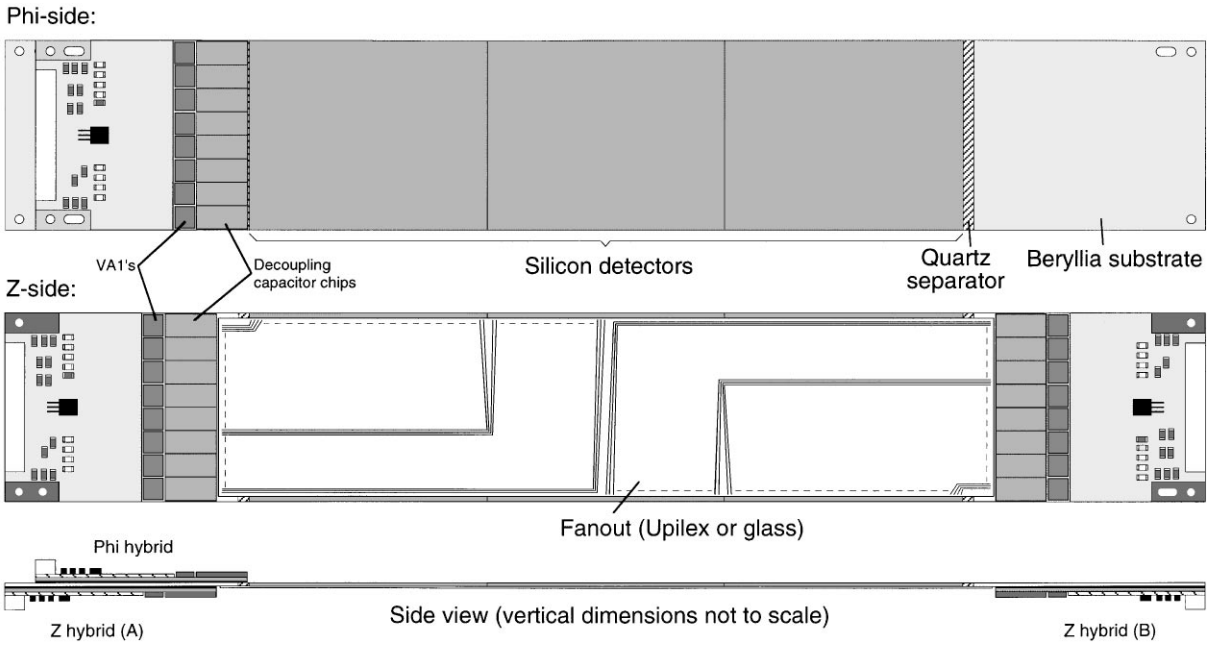

Fig. 1. Physical layout of the detector modules.

precision mounting systems under a Mitutoyo coordinate measuring machine. The active elements of the detector module are three 300 μm thick double-sided silicon microstrip detectors glued end-to-end. Quartz spacers, 300 μm thick and 5 mm long, are then glued at each end to increase as much as possible the thermal resistance between the hybrids and detectors. Beryllia ceramic pieces, which act as supports for the hybrids and conduct the heat away from the electronics, are then glued to the quartz spacers. The fanout is then glued to the detectors, and finally the hybrids are glued to the beryllia support pieces using an epoxy containing aluminium nitride for good heat conduction along with precision copper corner pieces which serve as both the mechanical and thermal interface between the module and its support flanges.

2.1. Silicon detectors

The silicon detectors are of identical design to those used in the ALEPH micro-vertex detector upgrade [3], and are produced by C.S.E.M., Neuchatel, Switzerland [4]. The physical pitch of the junction side strips is 25 μm but, taking advantage of capacitive charge division [5], every second strip is left unconnected resulting in a readout pitch of 50 μm which matches well with the readout electronics. All strips are biased from the common guard ring using the reach-through technique [6]. Each single detector has 1021 readout strips on the junction side, which are daisy-chained across the module using ultrasonic wire-bonding to a single readout hybrid. The strips on the ohmic side are orthogonal to those on the junction side. The n-type strips are on a pitch of 50 μm, electrical separation between them being achieved using p-stop implants between the readout strips. The strips are biased from the common n-type guard ring by shaping the naturally occurring electron accumulation layer at the oxide/silicon interface with careful design of the p-stops to create conductive channels with a typical resistance of 20–30 MΩ. Each single detector has 1280 n-type strips but, as for the junction side, only every second strip is physically connected to an amplifier and therefore the readout pitch is 100 μm. The connection between the strips and the readout electronics is made via a separate fanout piece which is glued directly to the ohmic side of the detector and then wire-bonded to the detector strips along the long side of the module and to the electronics readout hybrids which, for the ohmic side, are at both ends of the module.

2.2. Fanout

Two fanout options have been tested, 50 μm thick Upilex flexible substrates with gold-plated copper tracks produced at CERN [7] and 100 μm thick glass substrates with gold-on-chrome tracks produced by MIPOT [8]. For the modules using glass fanouts there are two separate fanout pieces, one for each readout hybrid, whereas the upilex modules have a single fanout piece that covers the entire length of the module. In no case is more than one strip connected to the same fanout track.

2.3. Naming convention

In the experiment the modules are mounted such that the junction side strips are parallel to the beam direction and therefore measure the phi coordinate in the r–ϕ–z cylindrical coordinate system; thus the junction side will be referred to from this point on as the "phi-side". Similarly, the ohmic side strips measure the z-coordinate in the r–ϕ–z cylindrical coordinate system and henceforth will be referred to as the "z-side".

2.4. Readout electronics

Three identical electronics hybrids, produced by IDEAS [16], are used in the construction of a single module, one for the phi-side readout and two for the z-side readout. Each hybrid has eight VA1 integrated circuits [9] providing a total of 1024 readout amplifier channels per hybrid. The VA1 integrated circuits are based on a low-noise, charge-sensitive preamplifier followed by a pulse-shaping circuit and then an analogue sample/hold circuit. The pulse shape seen at the input to the sample/hold is a close approximation of the impulse response of a standard RC–CR filter. Once the hold has been enabled, set by an input signal common to all channels and timed to correspond

to the peaking time of the amplifiers, the voltages of all the sample/hold circuits are read out sequentially to a buffered differential output. In addition, the VA1 is designed to be cascaded and so each hybrid has a single differential analogue output used to transmit the signal level of all 1024 channels to the data acquisition system. The strips are bonded (for the z-side via the fanout) to eight integrated decoupling capacitor chips on the hybrid which are then, in turn, bonded to the inputs of the eight VA1s. The decoupling capacitor chips, which are produced by CSEM with a design similar to that used for the ALEPH upgrade modules, prevent the leakage current of the strips interfering with the internal voltage levels of the amplifiers. Each decoupling capacitor has a typical value of 110 pF. The hybrid substrate is aluminium nitride, chosen for its high thermal conductivity, to which is glued a double-sided printed circuit for the electrical routing between the connector and the VA1s.

The complete readout chain can be seen in Fig. 2. Each hybrid is connected via a short flat cable (less than one metre in length) to a "repeater" card which, as well as regulating the necessary supply voltages for the hybrid, provides buffers for both the incoming hybrid digital control signals and the outgoing analogue readout signal. The repeater card is, in turn, connected via longer cables (up to ten metres long) to a decoupler card where both analogue and digital signals pass through opto-isolator circuits before being passed to/from the VME-based ADCs and readout control modules. This not only helps to decouple the extremely sensitive amplifiers of the hybrid from the electrical disturbances inevitably generated by the computer-based acquisition system but also allows the hybrid to float at the voltage of the strips to which it is connected and therefore eliminates the problems associated with maintaining the bias voltage across the decoupling capacitors on the hybrid.

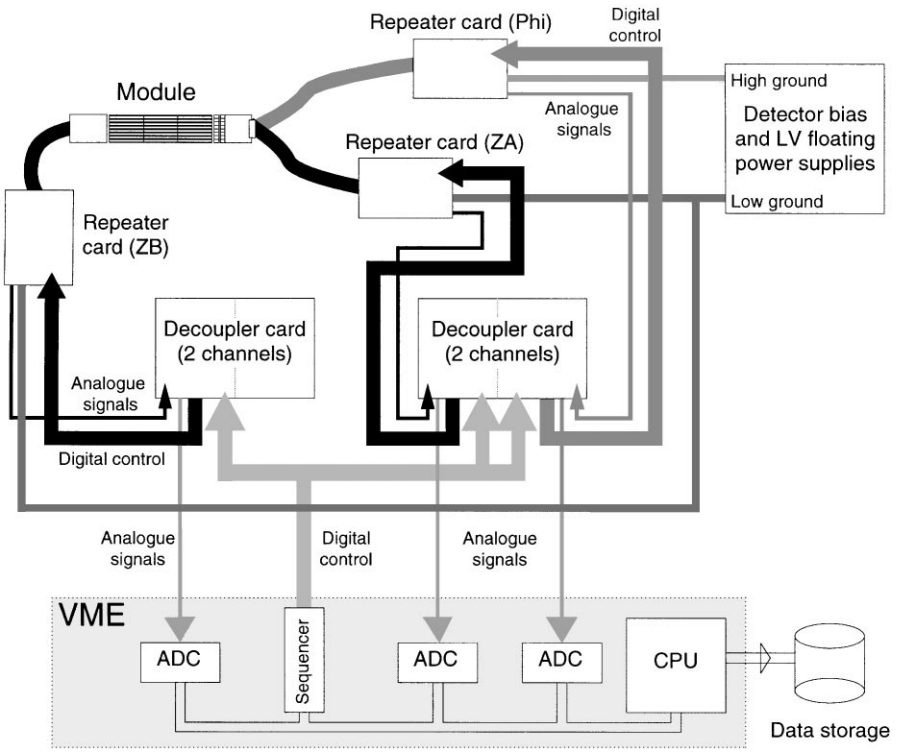

Fig. 2. Readout chain for the detector modules.

2.5. Data acquisition

The digital control signals necessary for triggering and clocking the readout of the hybrids are provided by a VME "sequencer" module, the V551b from CAEN [10], which generates readout control sequences in response to an external trigger and which also allows all important timing parameters to be programmed from the readout CPU. The VME ADC modules used are CAEN V550 2-channel 10-bit flash ADC modules which are designed to be driven by the V551b. Each hybrid has a dedicated ADC channel. The V550 design includes the possibility of data reduction using a programmable pedestal and threshold for each channel, but in the test described here the thresholds were set to zero such that the data from all channels were recorded for every event. In the test, the sequencer was programmed to use a clock time per readout channel of one microsecond. A CES FIC8234 34 MHz VME CPU was used to read out the ADCs with a "producer" program running under the OS-9 operating system. A second Digital Alpha-VME CPU running the OSF-1 operating system was used to run a "consumer" program to collect the data from the "producer", manage the storage of the data on an Exabyte tape drive, and to allow on-line checks of the data via an X-windows-based monitoring program.

3. Experimental setup

The test was carried out in the M11 beam line of the TRIUMF accelerator facility, Vancouver, Canada [11]. Fig. 3 shows the experimental setup in the beam line. The beam can be tuned to provide both pions and protons over a momentum range from 150 to 410 MeV/c. Absorbers of predetermined thicknesses in the mid-plane of the M11 channel make it possible to control the ratio of pions to protons in the trigger by varying the field of the last dipole of the channel. There is an unavoidable contamination of muons and electrons, but the geometry of the trigger system ensures that it is always less than 1% in the trigger sample.

For mixed beams a dedicated scintillator system trigger based on energy deposition was used to balance the number of pion and proton triggers. The coincidence of the three scintillators shown in Fig. 3 was used to trigger the module readout, thus ensuring that essentially all the triggered events contained a particle track passing through the active area of the module. The percentage of pions and protons in the beam was monitored by counting the number of particles, separated according to pulse height in the scintillators.

Three smaller double-sided silicon detector units (DSSDUs) were also used for tracking and independent energy measurements. It should be noted, however, that the tracking capability of this system with such a low-beam momentum is inevitably compromised by multiple scattering, with the error on the track projection to the module position substantially greater than the intrinsic resolution of the module itself.

The modules under test were mounted on a frame which allowed the rotation of the module on two axes with respect to the beam and data were taken at several different angles. All measurements

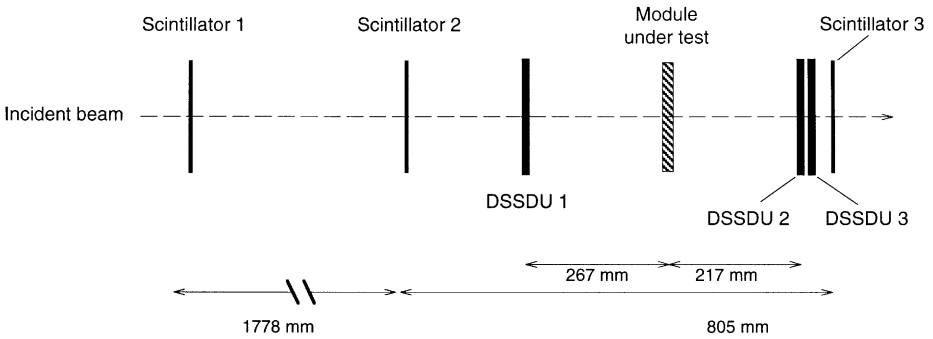

Fig. 3. Experimental setup for the test.

were made with both the Upilex and glass fanout modules. The results presented here will, however, be concerned only with the glass fanout module mounted such that the particles passed through the detector orthogonally with respect to both the phi- and z-side strip axes (it is planned to publish the complete data set at a later date). Two beam momentum settings were used, 408 MeV/c which provides pions close to minimum-ionising and protons similar to those produced in the decay of the hyper-nucleus, and 270 MeV/c which provides pions similar to the prompt pions from the hyper-nucleus decay and heavily ionising protons used to simulate the energy deposition associated with the kaons produced by the decay of the $\phi(1020)$ at rest. The peaking time for the VA1 amplifiers was set to 1.2 μs. Before commencing the bulk of the data taking, an initial set of timing runs was made to determine the correct trigger/hold delay.

4. Data analysis

4.1. Pedestals, common mode, and channel noise determination

Every readout channel has an associated voltage offset, commonly referred to as the channel "pedestal", which must be measured and subtracted from the ADC value in order to determine the signal on that channel. The raw data for any given channel contains, in addition to the irreducible stochastic noise, additional noise due to electrical disturbances and, occasionally, signals from particles crossing the readout strip. The noise due to electrical disturbances is often described as "common mode" because, in any given event, it is typically seen to be equal for a well-defined block of readout channels and therefore can easily be corrected for in a system with low hit occupancy. Every event is therefore also corrected for common mode.

4.2. Cluster charge

The algorithm used for cluster charge determination is based on standard techniques for silicon microstrip data analysis [12]. From the geometry of the trigger it can be assumed that there will always be one single-particle track within the detector for any given event. Thus a search is made for the active channel with the highest signal to noise ratio in the event. If that channel's signal to noise ratio exceeds 5 then it is considered a valid signal, at which point any neighbouring channels with a signal to noise ratio exceeding 2.5 are also added to make up the overall "cluster". The total signal of the cluster charge is then recorded for that event. If no valid signal is found then the event is discarded.

4.3. Particle track position

As already noted, the modules are read out in such a way that, for both sides of the detector, there is an unconnected ("floating") strip between each readout strip. Charge arriving on a readout strip is almost entirely read out by the amplifier to which it is connected, with the exception of a small amount coupled to neighbouring strips due to the fact that the decoupling capacitors are not infinitely large. However, charge arriving on a floating strip is read out via capacitive charge division, which involves a certain amount of charge loss due to, for example, the capacitance between the floating strip and the other side of the detector. In order to take into account these effects it is therefore important to know the particle track position. Without the possiblity of precision external tracking information it is necessary to use the properties of the detector itself. Thus the particle track position is obtained by calculating the barycentre of the charge distribution in the usual manner [12]. Although this barycentre is not linear with position, clean selection of events either close to the readout strip or close to the floating strip is possible since the eta distribution is flat in these regions.

4.4. Cluster shape

Typically in tracking applications, where only particles close to minimum ionising are of interest, the number of strips in the cluster is enough to describe the charge distribution. The use of capacitive charge division, however, causes the signal to be spread relatively widely, due to coupling between adjacent floating strips, and thus the number

of strips above threshold becomes particularly dependent on the signal/noise ratio. For minimum ionising particles, strips with a few percent of the total cluster charge will usually be below threshold, but, as the signals increase, more of these strips will be above threshold and therefore the cluster size will appear to increase even though the relative charge distribution remains unchanged. With the very large dynamic range dealt with in these measurements it is therefore necessary to define the cluster shape in such a way that it is independent of signal/noise considerations. For this analysis, the cluster shape is defined as follows. For each event, first the cluster charge is determined in the usual manner. The cluster charge barycentre is then calculated based on channel number (i.e. a barycentre of 23.0 means a hit position centred exactly on readout strip 23 whereas a barycentre of 45.5 means a hit position exactly half-way between readout strip 45 and readout strip 46, which also corresponds to the position of the floating strip between the two readout strips). The signals from all the channels within five channels of the cluster centre – regardless of whether the channels are above threshold or not – are then individually normalised to the total cluster charge in order to create the cluster shape for that event. Separate average cluster shapes are accumulated according to the fractional part of the event barycentre, and these are then interleaved in order to create the final overall cluster shape. For runs containing both pions and protons a simple cluster charge threshold is used to select clusters according to particle type. As will be seen in the results section, the emphasis of not using a threshold for the surrounding channels is important because this allows the noise to be averaged away.

4.5. Treatment of inefficient strips

The percentage of strips with problems was relatively high for these prototype modules and therefore studying the efficiency of the entire module is not of great interest. Instead, if the signal cluster for an orthogonal track is two strips or less distant from a strip with problems then that event is rejected from the analysis. In this way the statistics are reduced but the quality of the data is not compromised.

4.6. Correction of data due to signal saturation

During the data analysis it was discovered that there were problems of saturation at large signal values. Further investigation revealed that this saturation had occurred not in the VA1 preamplifier/shapers but in one of the two channels of the differential pair of the analogue decouplers, and only for large signals where most of the charge was collected on a single strip. Thus correction of the data is possible since, essentially, the overall gain is reduced by a factor of two beyond a certain ADC value. The only negative aspect to this correction is that the pickup rejection qualities of the differential pair are lost for the channels in saturation, and therefore the effective noise for the corrected signals is somewhat higher (it must be emphasised that this applies only to channels with signals above the saturation threshold). However, as will be seen, the natural energy spread of the energy deposition for the protons is wide enough to make this extra noise contribution almost negligible. All the results presented have been corrected for this saturation.

5. Results

5.1. Noise performance

The channel noise histograms for two hybrids, one phi-side and one z-side from the detector with the glass fanouts, are shown in Fig. 4. It is clear that the number of noisy channels is greater than would be acceptable for modules to be used in the experiment, due to a number of technical problems encountered in construction of these first prototypes. In addition, because these were the first prototypes, the highest quality detectors and fanouts were not used. The use of two hybrids at opposite ends of the module on the z-side causes this design to be unusually sensitive to power supply noise and residual pickup problems, however the levels achieved in the test were low enough to not cause any detectable degradation in performance after correction (comparison made with laboratory noise measurements at significantly lower common mode levels). Some degradation, however, in the overall noise

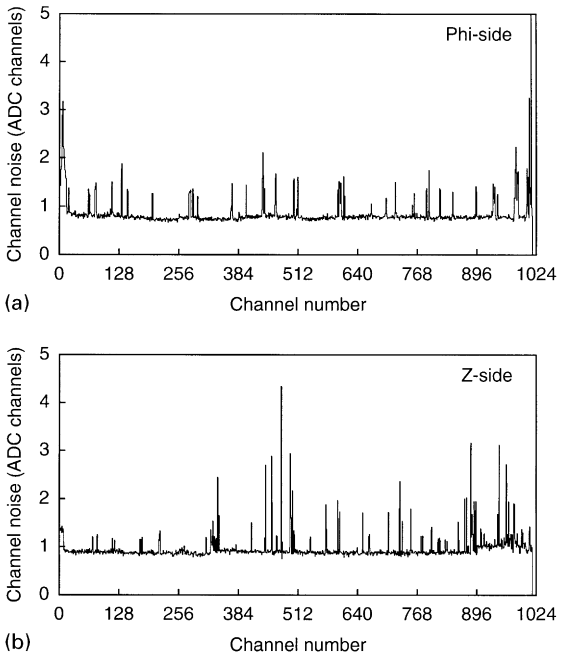

Fig. 4. (a) Phi-side channel noise. (b) Z-side channel noise.

performance was unavoidable due to the need to accommodate the extremely large signals generated by the protons at 270 MeV/c within the 10-bit ADC range. Reducing the gain caused the residual noise of the repeater buffer and decoupler electronics to become non-negligible, although low enough to not be the dominant contribution to the noise.

Defining the signal-to-noise ratio as the most probable signal value for the 408 MeV/c pions (for events where the particle passes directly beneath a readout strip) divided by the average single-channel noise, we obtain the following values:

S/N (phi) 24.3,

S/N (z) 20.7,

It must be emphasised that the energy deposition of these points is truly at the minimum of the energy deposition curve, 20–30% lower than that observed in particle beams with energies in the GeV range. Although the noise performance is more than adequate for the application, the values are lower than can be achieved with the VA1 with these loads. There are a number of reasons for this, including non-optimal leakage current levels, lower than standard current in the preamplifiers in order to minimise the power dissipation in the VA1s, and the reduced post-hybrid gain necessary to accommodate the large dynamic range. It is not clear, however, why the noise level is higher on the z-side than the phi-side, since, from simple geometrical arguments, both capacitance and leakage current noise contributions should actually be larger for the phi side. The z-side noise shows no obvious dependence of the fanout length, thus effects related to capacitance or series resistance of the fanout are ruled out. This appears to leave the accumulation layer biasing resistors as a physical cause, or, perhaps, some undetected systematic problem associated with the double-hybrid configuration of the z-side.

5.2. Overall charge deposition

Fig. 5 shows the cluster charge histograms for the different combinations of detector readout side and beam momentum. From Fig. 5a and b it can be seen that at 408 MeV/c there is some overlap in the two distributions due to the tail of the pion energy loss (see Section 5.6), whereas in Fig. 5c and d the separation at 270 MeV/c between pions and protons is very clear. Comparing the phi- and z-side data there is also an evident broadening of the cluster charge distribution for the z-side towards lower energies, becoming two resolved peaks for the protons at 270 MeV/c. This is due to the charge sharing readout scheme, and will be discussed in more detail in the next section. Fig. 6 shows the cluster charge correlation between phi- and z-side. Again the broadening towards lower energies is clear.

5.3. Charge loss due to floating strips

Fig. 7 shows the separated data based on selecting events using the barycentre value as described in Section 4.4. The value "B" is defined as the event barycentre subtracted from the number of the strip closest to the particle hit. The label "$B = 0.0$" is used to indicate an absolute value of "B" less than 0.125, thus corresponding to events where the

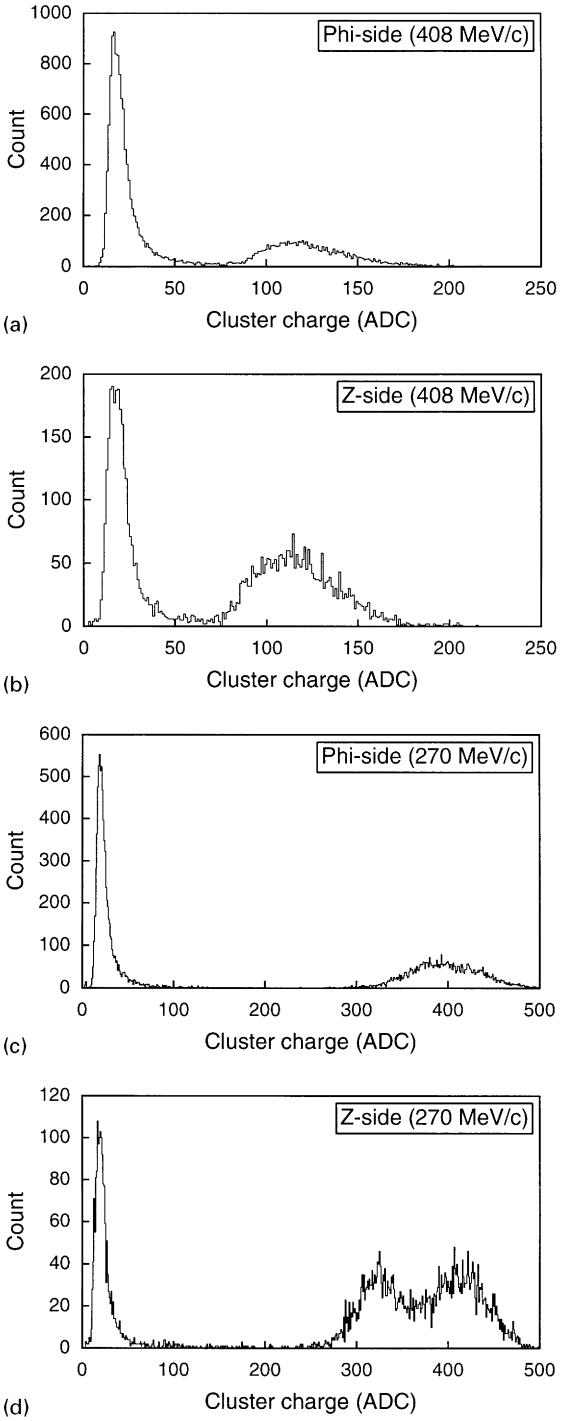

Fig. 5. (a) Phi-side cluster charge histogram, 408 MeV/c. (b) Z-side cluster charge histogram, 408 MeV/c. (c) Phi-side cluster charge histogram, 270 MeV/c. (d) Z-side cluster charge histogram, 270 MeV/c.

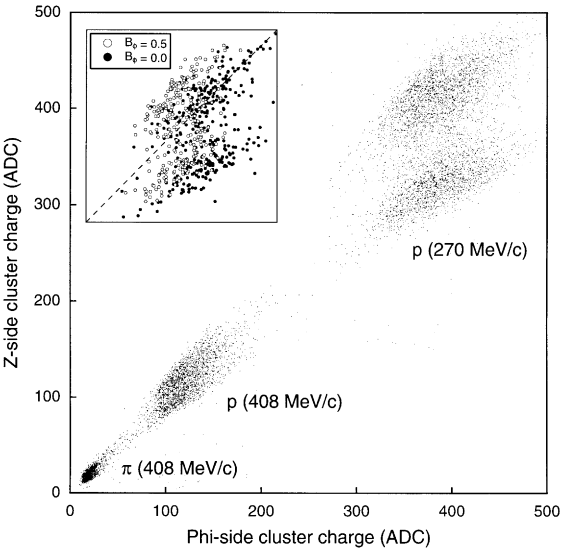

Fig. 6. Cluster charge correlation between phi-side and z-side, with inset containing a subset of the 270 MeV/c proton data selected according to phi-side barycentre.

charge is collected on the read-out strip, and "$B = 0.5$" is used to indicate an absolute value of "B" greater than 0.375, thus corresponding to events where the charge is collected on the floating strip between two readout strips. It can be seen that a clean selection of events is achieved even for the protons at 270 MeV/c. From Fig. 7a, the effect of charge loss for the floating strips is visible also for the phi-side. Thus there are actually four identifiable zones contributing to the correlation plots in Fig. 6 depending on whether or not charge loss has occurred for each side. To illustrate this more clearly, the inset in Fig. 6 shows a subset of the data for the 270 MeV/c protons plotted with different symbols according to the phi-side barycentre selection.

5.4. Cluster shape

Fig. 8 shows the histograms for the number of strips in the cluster. There is a clear difference between the different particles and momenta, but, as already discussed in Section 4.4, this is a natural result of the capacitive charge division readout. Fig. 9 shows the cluster shape, as previously

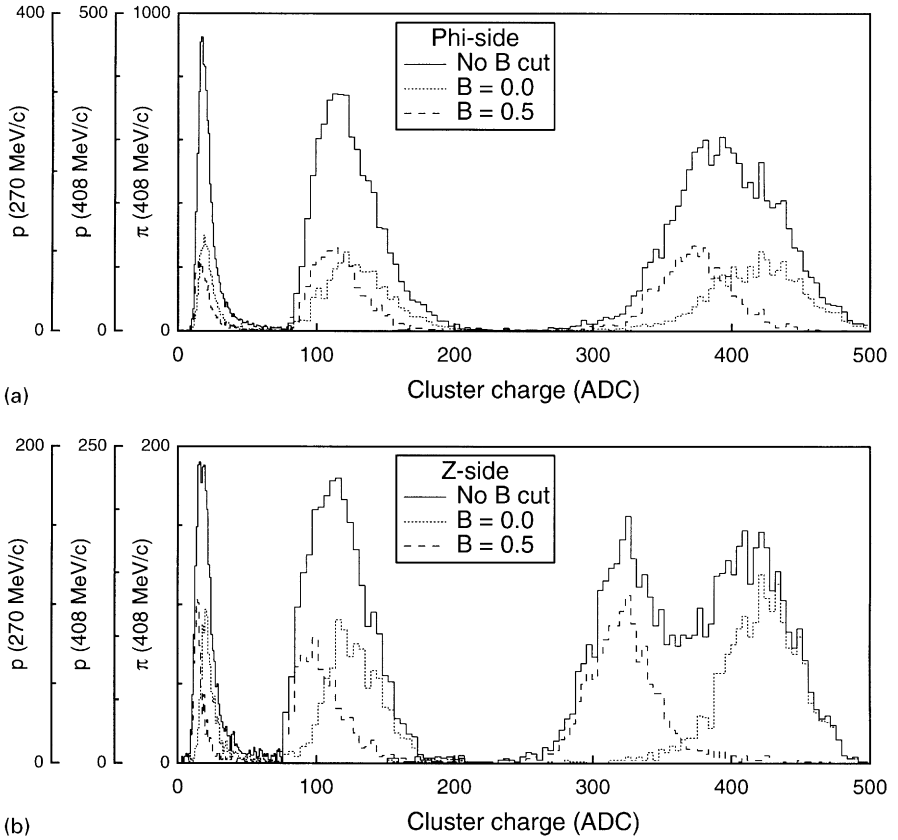

Fig. 7. (a) Phi-side cluster charge with selection based on the track barycentre. (b) *Z*-side cluster charge with selection based on the track barycentre.

defined, for the same data (when considering the spatial extent of the clusters in Fig. 9 it must be remembered that one strip corresponds to 50 μm on the phi-side and 100 μm on the *z*-side). Now it is seen that there is actually very little difference between pions and protons, with the averaging making the tails of the cluster charge distribution visible even for the pions. Comparing the phi-side and *z*-side cluster shapes there is a difference in the amount of charge collected on neighbouring strips, with the cluster being more spread out on the phi-side since the strip pitch is narrow enough to be comparable with the natural width of the charge deposition due to diffusion. The total strip capacitance on the phi-side is expected to be about twice that of the *z*-side (including the fanout) and therefore charge spreading due to the finite value of the decoupling capacitors will also be greater for the phi-side.

5.5. Energy resolution

The relative energy resolutions for the protons obtained from the cluster charge histograms are shown in Table 1. For the protons at 270 MeV/*c* the results are taken from a Gaussian curve fit, for the protons at 408 MeV/*c* a parametrised Landau curve fit was made and the resolution calculated as the full-width half-maximum of the fit divided by the peak value of the fit. Values are given both for the complete data and, in order to provide values independent of charge loss effects, for the data selected for barycentre "$B = 0.5$" (the choice of "$B = 0.5$" instead of "$B = 0.0$" for the barycentre

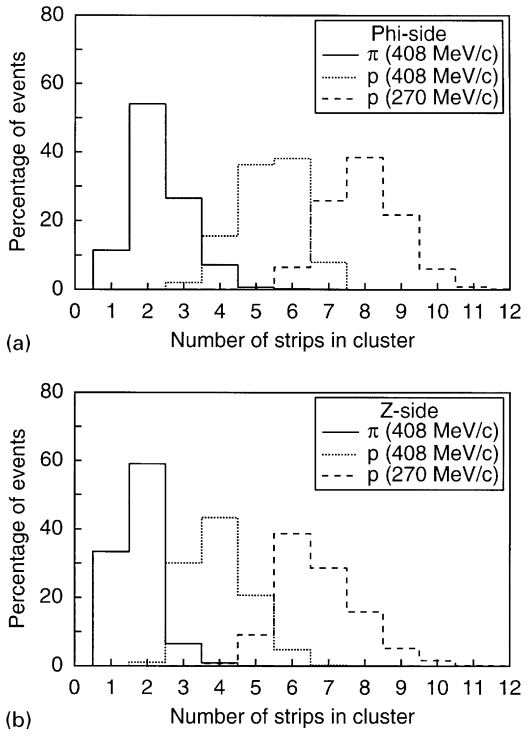

Fig. 8. (a) Phi-side cluster size. (b) *Z*-side cluster size.

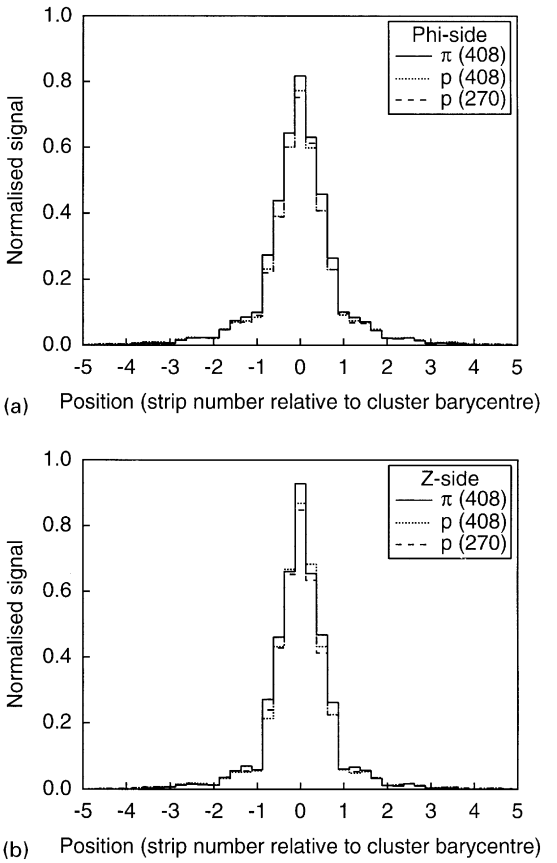

Fig. 9. (a) Phi-side cluster shape. (b) *Z*-side cluster shape.

cut is to ensure that there are no residual effects due to the saturation correction). Also shown in Table 1 are the equivalent values obtained from the GEANT simulation, which will be discussed in Section 6.

It is also interesting to consider the measurement of the pion energy deposition. As already seen from the cluster charge shape, there is a certain amount of charge which will inevitably be lost due to the effect of the threshold for neighbouring strips. If, however, the single-channel noise is low enough then it is also possible to simply sum the charge on the strips either side of the centre strip in the cluster – regardless of value – thereby ensuring improved charge collection at the expense of increasing the noise associated with the measurement. Fig. 10 shows the effect of the neighbour strip threshold on the cluster charge distribution for phi-side pion events with barycentre close to zero. For the simple strip sum it is observed that the peak of the distribution is shifted towards higher values while the shape of the distribution is actually slightly narrower, indicating also that the noise is not yet high enough to be a negative influence on the distribution.

Table 1
Relative energy resolution based on cluster charge histograms, measured from data and from GEANT simulation

	No barycentre cut		$B = 0.5$	
	Data (%)	GEANT (%)	Data (%)	GEANT (%)
408 MeV/*c*				
Phi-side	40	35	36	30
Z-side	47	48	36	31
270 MeV/*c*				
Phi-side	24	22	15	16
Z-side	*	*	15	15

*Distribution too distorted to allow a meaningful curve-fit.

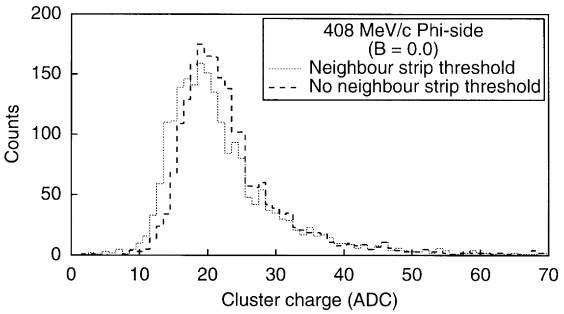

Fig. 10. Cluster charge distribution for 408 MeV/c pions, phi-side, barycentre 0, with and without neighbour strip threshold.

Table 2
Percentage of phi-side events at 408 MeV/c, selected for particle type, below various thresholds of energy deposition

Threshold (keV)	Data (408 MeV/c)		GEANT (408 MeV/c)	
	Pions (%)	Protons (%)	Pions (%)	Protons (%)
170	90.0	0.0	91.5	0.0
235	95.0	0.0	96.6	0.0
350	98.0	0.0	99.2	0.0
430	99.0	7.1	99.6	4.6

5.6. Mass discrimination

Using the energy deposition measured in the DSSDU's for particle identification it is also possible to study directly the discrimination between pions and protons based on the experimental data. At 270 MeV/c the separation is so large that no misidentifications are found. At 408 MeV/c there is some natural overlap due to the Landau tail of the pion energy distribution. To demonstrate this, Table 2 shows the percentage of the total particle-identified events which release less than a certain amount of energy in the phi-side of the module (the energy lost in the module is determined from the total cluster charge assuming 26 keV/100 μm as the most probably energy release for a minimum-ionising particle in silicon). For comparison, Table 2 also shows the equivalent results from the GEANT simulation. It can be seen that with a threshold of 350 keV, chosen to correspond to 98% of the pion distribution, there are no misidentifications. Approximately 1.5% of the pions are found within the range of the proton distribution, which begins at about 370 keV.

6. Comparison with GEANT

Since Monte-Carlo simulations are very valuable for studying the response of the detector apparatus independently of the physical hardware, it is important to know how reliable those simulations are. GEANT [13] was used to simulate the test beam setup. The experimental layout was simulated, as well as the real beam composition and divergence. The GEANT parameters were chosen to explicitly generate delta-rays production (LOSS = 1, DRAY = 1), similarly to previous works which treated the interaction of particles with silicon microstrip detectors [14]. After calculating both the amount and the spatial distribution of the energy deposited in the silicon detector, the program simulated the drift and lateral diffusion of the electrons and holes created in order to calculate the charge induced on each strip [15]. Finally, the charge was distributed to the preamplifiers, taking into account the different effects of the capacitive charge division for the floating and non-floating strips. Noise in the preamplifiers was simulated using a simple Guassian distribution, without taking into account channel correlation effects. Fig. 11, combined with the values in Table 1, shows that the simulation reproduces the results generally well, although it is noted that the distribution for the protons at 408 MeV/c is slightly wider for the real data than for the simulations. Considering the results in Table 2, it is also seen that the high-energy tail of the pions is statistically less significant in GEANT, with only 0.8% of pions above 350 keV and 0.4% above 430 keV instead of 2% and 1%, respectively, from the measured data.

7. Conclusions

Silicon microstrip detectors combined with low-noise VA1 electronics designed for precision tracking applications have been demonstrated to be

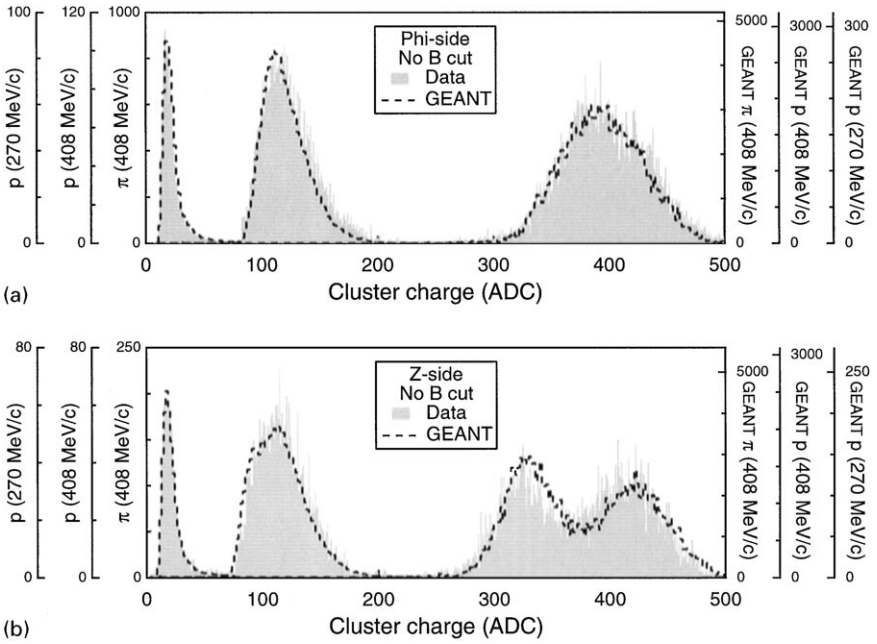

Fig. 11. (a) Phi-side cluster charge distributions from data and GEANT simulations. (b) *Z*-side cluster charge distributions from data and GEANT simulations.

well-suited also to the application of mass discrimination at intermediate energies. The only limitation to the performance in this application is the natural width of the particle energy deposition in silicon. With careful choice of operation parameters the dynamic range of this system can accommodate signals 20 times greater than those from minimum ionising particles. The use of floating strips results in some complications in the data analysis, most notably the apparent widening with increasing energy deposition of clusters defined with fixed thresholds, but the choice of appropriate algorithms demonstrates that the only substantial differences in the detectors' response to the various particles and energies come simply from the different effective signal/noise ratios.

Acknowledgements

We would like to thank the following people for their invaluable efforts in helping to prepare for and carry out this work: Roberto Baccomi for the layout of the glass fanouts, for the design of the tools used for gluing the hybrids to the modules and of the tools for supporting the modules during the bonding process. Michele Sacchetti for the design of the optical decoupler, and the layout of the Upilex fanouts. Piero Vasta for the gluing of the modules, and for the design of the module supports used in the test beam. We thank the mechanical and electronic support staff at Trieste and Bari for their contributions to the construction and testing of the various pieces. In addition we are grateful to the director and staff of TRIUMF for providing access to the beam facilities. Finally, we thank Luciano Bosisio for his help with the module design and detector testing.

References

[1] M. Agnello et al., The FINUDA Collaboration, "FINUDA Technical Report", LNF publication LNF-95/024 (IR), 1995.
[2] Proposal for a ϕ-factory, the ϕ-factory Study Group, Frascati Report 90/031 (R), 1990.
[3] E. Focardi, Nucl. Instr. and Meth. A 386 (1997) 18.
[4] Centre Suisse d'Electronique et de Microtechnique SA, Neuchatel, Switzerland.

[5] J.B.A. England et al., Nucl. Instr. and Meth. A 185 (1981) 43.
[6] J. Kemmer, G. Lutz, Nucl. Instr. and Meth. A 273 (1988) 588.
[7] Product Engineering and Support Group, CERN, Geneva.
[8] MIPOT S.p.A., Cormons (GO), Italy.
[9] O. Toker et al., Nucl. Instr. and Meth. A 340 (1994) 572.
[10] Costruzioni Apparecchiature Elettroniche Nucleari S.p.A., Viareggio, Italy.
[11] 1987 TRIUMF Users Handbook, TRIUMF, Vancouver, Canada.
[12] For example, R. Turchetta, Nucl. Instr. and Meth. A 335 (1993) 44.
[13] GEANT, A Detector Description and Simulation Tool, part of the CERN Program Library (http://wwwinfo.cern.ch/asd/).
[14] S.R. Hou et al., Nucl. Instr. and Meth. A 386 (1997) 186.
[15] E. Gatti, P.F. Manfredi, La Rivista Nuovo Cimento, 9 (1) (1996) 20.
[16] Integrated Detector and Electronics AS, Høvik, Norway.